Fuel 335 (2023) 127017

Contents lists available at ScienceDirect

Fuel

journal homepage: www.elsevier.com/locate/fuel

Full Length Article

Emissions from a Euro 6 engine using polyoxymethylene dimethyl ethers: Chemical effects vs mapping strategy

Silvana Arias [a,b], John R. Agudelo [b], Angel Ramos [c], Magín Lapuerta [c,*]

[a] Grupo de Investigación en Gestión y Modelación Ambiental-GAIA, Escuela Ambiental, Facultad de Ingeniería, Universidad de Antioquia UdeA, Calle 70 No. 52-21, Medellín, Colombia
[b] Grupo de Manejo Eficiente de la energía GIMEL, Facultad de Ingeniería, Universidad de Antioquia UdeA, Calle 70 No. 52-21, Medellín, Colombia
[c] Escuela Técnica Superior de Ingeniería Industrial, University of Castilla – La Mancha, Edificio Politécnico, Avda. Camilo José Cela, s/n., 13071 Ciudad Real, Spain

ARTICLE INFO

Keywords:
Electrofuels
Diesel engines
OME
Combustion
Emissions

ABSTRACT

New fuel technologies, such as electrofuels, are an attractive alternative to meet the energy demand and emission regulations, with sustainable electricity being the primary source of energy. Recently, there is increasing interest in using polyoxymethylene dimethyl ether (OME) as a diesel substitute. This study investigated the effect of a diesel fuel blend with 20% of OME (OME20) with 3–5 oxymethylene groups, on the performance, combustion characteristics, regulated emissions, particle number (PN), and particle size distribution in a compression ignition Euro 6 engine following the Worldwide harmonized Light vehicle Test Cycle (WLTC). Regulated emissions were measured downstream of the aftertreatment system, while PN emissions were measured upstream of the particulate filter. The results showed that OME20 increased the peaks of pressure and heat released rate, causing an increase in the combustion speed compared to diesel. OME20 reduced CO and THC accumulated emissions by 52% and 17%, respectively, and the PN exhibited a dramatic reduction close to 61%. Such reductions were influenced by both the fuel formulation and the engine settings induced by the fuel. With OME20, the engine requires higher fueling to maintain the same power output. Therefore, the accelerator pedal position was higher compared to diesel, leading a decrease in exhaust gas recirculation (EGR) rate to increase the air mass flow. Consequently, PN, CO and THC emissions were reduced, and conversely, accumulated NO_x emissions increased up to 42%. OME20 decreased the peak number concentrations of accumulation-mode particles at all driving cycle phases and caused a slight shift of the particles toward smaller size compared to diesel fuel. From the results, it can be concluded that PN and regulated emissions, despite being strongly affected by the fuel properties, are very sensitive to the EGR rate and the equivalence ratio, which are established in the engine mapping.

1. Introduction

The tight supply of crude oil and the need to achieve net-zero greenhouse gas emissions have prompted the search for new alternative fuel sources. Oxygenated fuels are promising alternative fuels due to their availability and their well-known impact on regulated emissions, especially the reduction of particulate matter (PM). Among various oxygenates, alcohols, esters and ethers are the three major categories that might serve as engine fuel components. Short and long chain alcohols have been widely investigated. However, although alcohols, either long-chain or short-chain could achieve the target of reducing PM with respect to diesel fuels, some disadvantages have been reported such as their low heating values, miscibility problems, and lower cetane numbers, higher NO_x emissions, and starting difficulties at very low ambient temperatures for higher blends [1–4].

Electrofuels (or e-fuels) are gaseous or liquid fuels which can be used in internal combustion engines. They are produced from hydrogen and captured carbon dioxide using renewable electricity as the power source [5]. New oxygenated e-fuels are being developed for use in internal combustion engines and may contribute to the decarbonization of transport. Polyoxymethylene dimethyl ethers (OME) are promising e-fuels for diesel engines because they contain nearly 50 % oxygen and have high cetane number. They are characterized by a CH_3–O–$(CH_2$–O$)_n$–CH_3 general structure, with n as the number of oxymethylene groups. Long chain OME ($n > 3$) have proven to be suitable for diesel engine applications due to their physical properties [6]. The viscosity,

* Corresponding author.
E-mail address: magin.lapuerta@uclm.es (M. Lapuerta).

https://doi.org/10.1016/j.fuel.2022.127017
Received 9 September 2022; Received in revised form 8 November 2022; Accepted 27 November 2022

Table 1
Regulated emissions trends and BTE for OME with respect to diesel fuel.

Ref	Engine	Blends	Operation mode	Results				
				PM	CO	NO_x	THC	BTE
[11]	Four-cylinder turbocharged intercooled common-rail diesel engine. 4.09L	0, 10 %, 20 % and 30 % of OME_{3-8} -Diesel	25 %, 50 %, 75 % and 100 % of engine load	↓ (27.6 %, 41.5 % and 47.6 %)	↓	↑	↓	↑
[12]	Single-cylinder research engine retrofitted from a four-cylinder common-rail compression ignition engine. 0.5 L and six-cylinder HD diesel engine	0, 10 %, and 20 % of OME_{3-4} -Diesel	At 2, 4 and 6 bar IMEP	↓ (Smoke opacity)	↓	↑	↓	↑
[16]		20 % of OME_{3-4} -Diesel	ESC test cycle	↓ (Smoke opacity)	↓	↑	↓	↑
[17]		Diesel Biodiesel 15 % of OME_{3-4} -Biodiesel	1600 r/min – 0.4 MPa, 0.6 MPa, 0.8 MPa, 0.9 MPa and 1.0 MPa	↓	↑ (at low load)↓ (at high load)	↓ (at low load)↑ (at high load)	↑	↑
[18]	Single-cylinder DI diesel engine based on a MTU 396 series engine common-rail	OME-Diesel 5 %, and 10 % of OME_{2-7} -Diesel	1050 r/min – 8 and 10.5 bar.	↓ (Smoke opacity)	↓	↑	N.A.	≈
[15]	Single cylinder engine. 0.39L	35 % OME_1-Diesel 35 % OME_2-Diesel 35 % OME_3-Diesel 35 % OME_4-Diesel 35 % OME_{3-5} diesel	4.3 bar 1500 r/min 6.8 bar 1500 r/min 9.4 bar 2280 r/min 14.8 bar 2400 r/min 16 bar 1400 r/min	↓	↓	N.A.	↓	≈
[19]	Four-cylinder, turbocharged, water-cooled, common-rail diesel engine. 2.7 L	0, 10 %, and 20 % of OME_{3-8} -Diesel	1600 r/min and 100 % engine load	↓	↓	↑	↓	N. A.
[14]	L12 small agricultural diesel engine	25 % of OME_{3-5} -Diesel	1800 r/min – 1 kW, 2 kW, 3 kW, 4 kW and 5 kW.	↓ (Smoke opacity)	↓	↓ (NO)	N.A.	N. A.
[20]	Four-cylinder, four-stroke, turbocharge, intercooled, common-rail diesel engine. 4.2 L	0, 10 %, 20 % and 30 % of OME_{3-6} -Diesel	2400 r/min – 0 %, 25 %, 50 %, 75 % and 100 % engine load	↓ (Smoke opacity) ↓ (PN)	N.A.	N.A.	N.A.	N. A.
[21]	Single-cylinder diesel engine, common-rail	2 %, 4 %, 6 %, 8 % 10 % of OME_3-Diesel	1200 r/min – 30 %, 40 %, 50 %, 60 %, engine load	≈	N.A.	↑	↑	N. A.
[13]	Six-cylinder in-line Weichai WP12.460 heavy-duty diesel engine, turbocharged and intercooled. 11.59 L	0, 10 %, 20 % and 30 % of OME_{3-6} -Diesel	1900 r/min, – 25 %, 50 %, 75 % and 100 % engine load	↓↓ (PN)	↓	↓	↓	↑
[22]	Six-cylinder, 24-valve, water-cooled, turbocharged heavy duty diesel engine, common rail injection system.	0, 15 % and 25 % OME_{3-6} -Diesel	WHSC test cycle	↓	↓	↓	↓	↓
[23]	AVL 501 single cylinder engine 2.13 L, equipped with a cylinder head from a Volvo D13 and a Ricardo Hydra engine 0.49 L, equipped with a Volvo NED4 cylinder head.	7 %, 18 % and 65 % OME_{3-5}–7% biodiesel- 10 % 2-Ethylhexanol and HVO	0.64 MPa 1200 r/min 1.11 and 1.61 MPa 1500 r/min 1.40 MPa 1800 r/min 0.8 MPa 1280 r/min 0.72 MPa 1810 r/min 1.1 MPa 2000 r/min	↓	N.A.	↑	N.A.	↑

*N.A.: Not available. The symbols ↓/↑shows the trend of variations obtained in each study. PN: Particulate number.

lubricity, vapor pressure and flash point are significantly improved with *n* ranging between 3 and 5 [7], and are miscible with diesel at any ratio without changing the structure of the diesel engine (drop-in fuel) [6].

There are several routes for the OME production via different intermediate steps. All technologically viable routes currently start from methanol. One of the most studied routes for the large scale OME production was described by Burger et al. [6,8], in which OME is formed from the intermediates methylal (dimethoxy methane) and trioxane. Methylal can be produced on a large scale by a pressure-swing process from formaldehyde and methanol [6,9]. The OME production costs are strongly dominated by the raw material costs. The economy of the process chain in OME production was assessed by Schmitz et al. [10], analyzing the influence of the price of methanol and the investment costs. Over a wide range of the price of methanol and the investment costs, they concluded that the production of OME is competitive or even cheaper than conventional diesel fuel production.

Recent studies investigating the effect of OME blending ratio on the performance and regulated emissions of diesel engines are summarized in Table 1. Researchers revealed meaningful reductions in soot emissions in the raw exhaust gas, due to the oxygen content and to the absence of C—C bonds. In some articles a reduction of NO_x emissions was observed [11,12], while in others an increase was reported [13,14]. Most published studies have been performed at steady state engine condition. Instead, transient operation is more likely to provide realistic results since the main impact on emissions is observed during accelerations, considering that engine load and speed change frequently during driving cycles. Few studies have been published following cycles for heavy-duty diesel engines, and to the authors' knowledge, this is the first using OME under driving cycle for light-duty vehicles. Furthermore, according to the literature, only a few investigations were found reporting the effect on particle size distributions [11,15].

The aim of this study was to evaluate the effect of a diesel fuel blend with 20 % of OME (with major content of $n = 3$–5) on the performance and pollutant emissions (CO, NO_2, NO, THC) in a compression ignition Euro 6 engine under transient realistic conditions. The tests were carried out following the Worldwide harmonized Light vehicle Test Cycle (WLTC) starting from cold-engine conditions. Furthermore, due to the links between PM emissions and health effects, measurements of particle number (PN) and particle size distribution were also performed.

2. Methodology

2.1. Experimental setup and engine

The experiments were carried out in an automotive, common rail direct injection, turbocharged and intercooled diesel engine, with Euro 6 technology manufactured by Nissan, model K9K (1.5 dCi). The engine was equipped with two exhaust gas recirculation loops, a low pressure

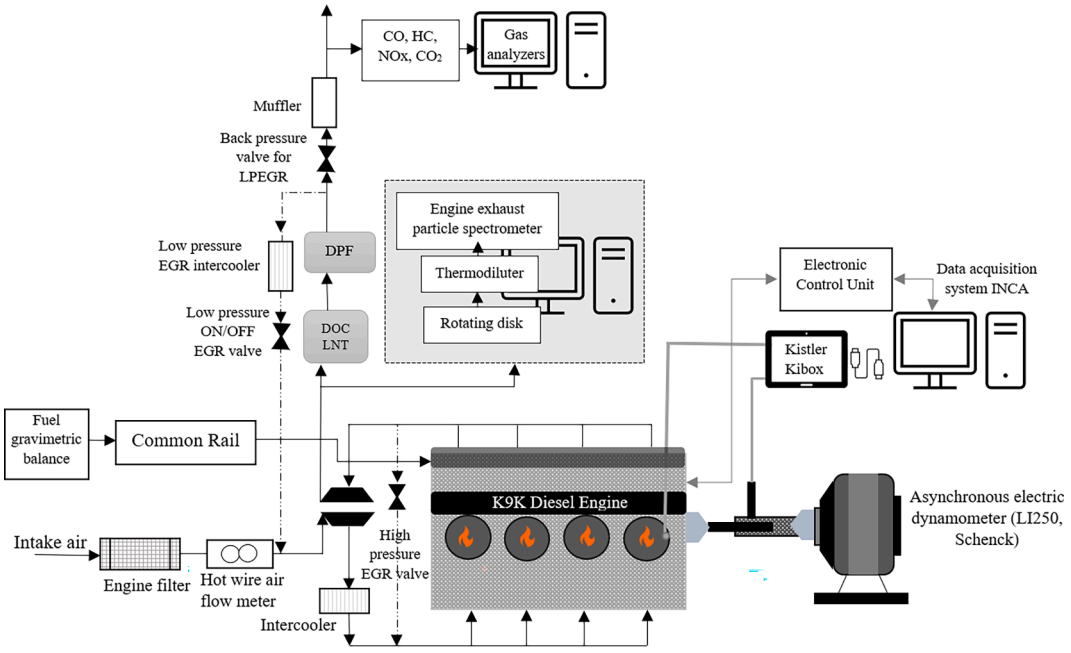

Fig. 1. Experimental installation for engine tests.

Table 2
Engine characteristics.

Cylinders	4 (in line)
Valves/Cylinder	2
Displacement (cm^3)	1461
Stroke (mm)	80.5
Bore (mm)	76
Compression ratio	15.5:1
Injection	Common rail direct injection
Torque (max.)	260 Nm/1750–2500 r/min
Power (max.)	81 kW/4000 r/min
After treatment system	DOC + DPF + LNT

Table 3
Characteristics of the simulated vehicle.

Transmission	Manual, 6 gears	Differential ratio	4.13:1
Vehicle test mass (kg)		1470	
1st:2nd:3rd:4th:5th:6th gear ratio		3.73:1; 1.95:1; 1.23:1; 0.84:1; 0.65:1; 0.56:1	
Coast-down parameters $F\,(N) = f_0 + f_1 V\,(km/h) + f_2 V\,(km/h)^2$		$f_0 = 89.6$; $f_1 = 0.0659$; $f_2 = 0.0391$	

cooled (LP-EGR) loop and a high pressure (HP-EGR) uncooled one, both loops never being active simultaneously. It was also equipped with a diesel oxidation catalyst (DOC), a Lean NO_x Trap (LNT) and a regenerative wall-flow-type diesel particle filter (DPF) located downstream of the DOC and the LNT. The experimental installation is shown in Fig. 1.

The resistive load, speed and torque of the engine was simulated and controlled by an asynchronous electric dynamometer (Schenck Pegasus Gmbh, Dynas model, LI250). The speed was taken from a digital tachometer attached to the rotor with an accuracy of ± 1 r/min. The torque was measured from a torque meter cell and a signal conditioner from Gesellschaft für Industrieforschung GmbH, GIF, with an accuracy of ± 0.1 %. Finally, the accelerator position was controlled from the control and power module LRS 2003. This module acts over the accelerator sensor, which is connected to the Electronic Control Unit (ECU) of the engine. A Road Load Simulation (RLS) system from Horiba was used to emulate powertrain and body of a Nissan Qashqai 1.5 dCi vehicle. The main characteristics of the engine and simulated vehicle are listed in Table 2 and Table 3, respectively. The experiments were carried out following the WLTC driving cycle.

In this work, the fuel and air consumption were measured with the original engine sensor (previously calibrated with an AVL 733 s fuel gravimetric system) with an accuracy of ±0.12 % full scale (FS) and hot-wire sensor, respectively. The data were registered with the INCA PC software. The regulated gaseous emissions (CO, CO_2, THC and NO_x = NO + NO_2) were measured at the tailpipe with a gaseous emissions analyzer (Envea) with an accuracy of ±1 % FS for THC ($ppmC_1$), NO_x (ppm) and ±0.5 % FS for CO, CO_2 (% v/v). The total hydrocarbon emissions (THC) were measured with a flame ionization detector Graphite 52M-D. Carbon monoxide and carbon dioxide emissions were measured with a non-dispersive infrared (NDIR) detector MIR 2M. The infrared beam goes through an optical filter to differentiate between CO and CO_2 before passing through the sample. NO_x emissions were measured using a chemiluminescence Topaze 3000 analyzer.

Solid particle emissions were measured upstream of the DPF with the Engine Exhaust Particle Sizer (EEPS) spectrometer model 3090 from TSI. A first dilution with air was carried out on a rotating disc (RD) model MD19-2E at 150 °C to avoid hydrocarbons condensation. After, when reaching 300 °C, the diluted exhaust gas was introduced in the evaporating tube of the thermal conditioner (TC) model ASET15-1. The aerosol flows into a mixing chamber for the second dilution to cool down its temperature. Primary dilution factor at RD was 107:1 and secondary dilution factor at the TC was 6.7:1, leading to a total dilution factor of 717:1.

Solid PN measurement upstream of the DPF made it possible to determine the effect of OME20 on engine emissions (independently of aftertreatment system) and on DPF regeneration frequency, and consequently on fuel consumption, and on NO_x trap life cycle [24].

For the thermodynamic combustion diagnosis, a Kistler Kibox instrument was used. In-cylinder pressure was measured with a piezoelectric pressure transducer (model 6056AU20, Kistler) coupled to a charge amplifier (5011B, Kistler). The crank angle signal was obtained with the original engine sensor. Using both signals the energy conservation equation was solved from in-cylinder experimental data providing characteristic parameters of the combustion process.

Table 4
Physicochemical properties of diesel, OME and blended fuel.

Property	Units	Method	OME	Diesel	OME20
Mean molecular formula	–	–	$C_{5.62}H_{13.5}O_{4.39}$	$C_{14.61}H_{27.38}$	$C_{11.91}H_{23.5}O_{1.29}$
C content	%wt	–	43.8	86.23	76.29
H content	%wt	–	8.8	13.77	12.62
O content	%wt	–	45.4	–	11.07
Molecular weight	kg/kmol	–	151.38	203.09	187.55
Stoichiometric air/fuel ratio	–	–	6.28	14.76	12.71
Derived cetane number	–	EN 16,715	69.40	52.56	54.65
Density	kg/m^3	EN 3675	1057.6	826.6	872.8
Viscosity	cSt	EN 3104	1.08	3.0	2.2
Lubricity	μm	EN 12156–1	330	428.9	330.9
Lower heating value (LHV)	MJ/kg	ASTM D240	19.36	42.895	38.14
Lower heating value	MJ/L	–	20.4	35.5	33.2
Cloud point (CP)	°C	EN 3015	−35	−33	−10.6
Flash point	°C	EN 2719	76.0	74	63.5
Cloud filter plugging point (CFPP)	°C	EN 116	−38	−34	−30

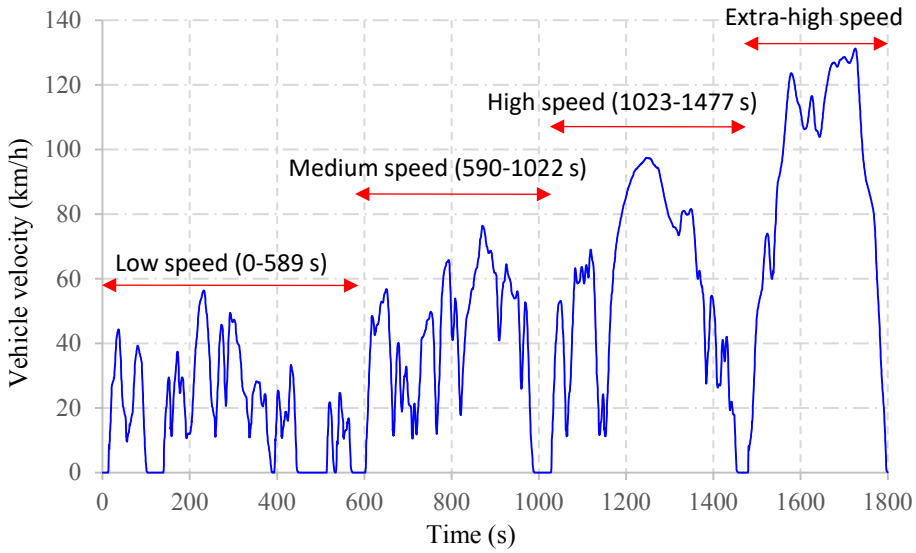

Fig. 2. WLTC driving cycle.

2.2. Test fuels

Two fuels were tested: 20 % OME by volume and 80 % diesel (OME20) and neat fossil diesel supplied by Repsol (Spain) as reference fuel. The OME content in the mixture was selected trying to avoid a significant loss of heating value (derived from its high oxygen content) and thus of vehicle fuel economy. In addition, miscibility and cold flow properties problems have been reported with blending ratios higher than 20 % of OME [11,15]. OME fuel was supplied by ChemCom Industries B.V- Netherlands, with a purity of 98.7 %. The OME fuel tested had different degrees of polymerization (*n*) i.e., 3, 4, 5, and 6, and their mass fractions were 57.24 %, 28.49 %, 10.61 %, and 2.34 %, respectively. The physical and chemical properties of the test fuels are shown in Table 4. It can be observed that the CFPP value.

According to the European standard EN 590, OME20 fulfils most of the limits proposed for diesel fuels. The high CP result for OME20 shown in Table 4 indicates that this blend would likely become immiscible at temperatures below −10 °C, as previously reported in [15]. However, the selected blend remained stable at −10 °C (usual temperature in European countries in winter), as tested following the protocol established in [25].

2.3. Test procedure

The WLTC was selected as driving cycle (Fig. 2). This includes four driving sub-cycles, whose details are presented in Table 5.

Table 5
Details of the WLTC selected in the engine tests.

Phase	Duration s	Stop duration s	Distance m	Maximum speed km/h
Low	589	156	3095	56.5
Medium	433	48	4756	76.6
High	455	31	7162	97.4
Extra-high	323	7	8254	131.3
Total	1800	242	23,266	

The tests were started from cold-engine conditions (19 °C), performed without any interruption, and repeated at least four times for diesel and OME blend at different days to evaluate the repeatability of the test and the results were averaged. The range of error corresponds to 90 % confidence intervals and were shadowed around the average values. Preconditioning test, including LNT regenerations, were always performed the day before each test, to ensure that the initial conditions did not change from one test to another. DPF regeneration and fuel filter change were performed before each fuel tests.

3. Results

Hereinafter, the engine parameters and the regulated emissions are

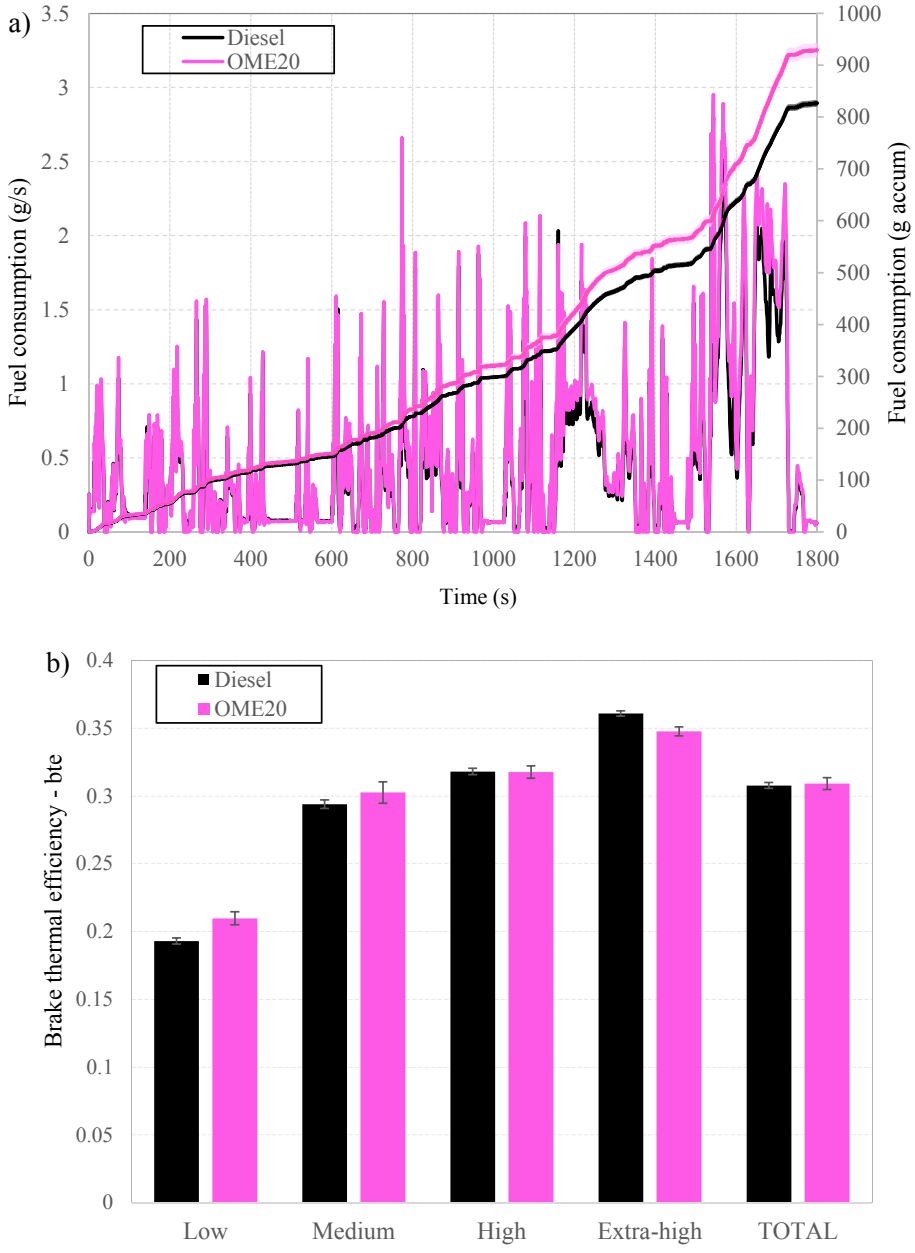

Fig. 3. Fuel consumption (a) and brake thermal efficiency (BTE) (b) of the tested fuels.

first presented and then the differences found between fuels are discussed.

3.1. Engine performance

Fig. 3a shows the instantaneous fuel consumption. Sharp consumption peaks were associated with accelerations for both fuels. At the end of the driving cycle, the accumulated fuel consumption was 11 % higher for OME20 compared to diesel (929 and 826 g, respectively), equivalent to the same percent decrease (11 %) in the LHV of OME20 with respect to diesel. This is due to the oxygen content in the blend (11 %) and implies that the engine would require more fuel to maintain the same power output. At idle and low load no significant differences were observed, while for high and extra high-speed phases, the higher consumption for OME20 became evident.

Average values of brake thermal efficiency are shown in Fig. 3b for each driving cycle phase. As expected, the worst efficiency was observed in the first phase for all fuels, when the engine was cold [11,26]. As the driving cycle progressed, the brake thermal efficiency (BTE) increased as a result of the higher engine temperature, and the reduction in mechanical losses. The BTE was slightly higher for OME20 than for diesel fuel in the low and medium-speed driving cycle phases. This increase can be explained because the OME intramolecular oxygen increased the combustion velocity, as detailed below. However, as the driving cycle advanced, the BTE was not significantly affected by the type of fuel, and in the extra high-speed driving cycle phase, diesel shows a slightly higher efficiency than OME20 due to a second regeneration of the LNT system, which occurred only for this fuel blend, as a consequence of its higher ECU-modelled NO_x emissions (see Section 3.3). The total BTE at the end of the driving cycle was not significantly different between fuels because the high efficiency for OME20 at the initial driving cycle phases was compensated by the low efficiency at the extra high-speed phase.

Exhaust pollutant emissions were markedly affected by the equivalence ratio and the EGR rate. Slight increases in both equivalence ratio and EGR led to sharp increases in CO, THC and PN emissions, which are not attributable to differences in fuel formulation. The instantaneous

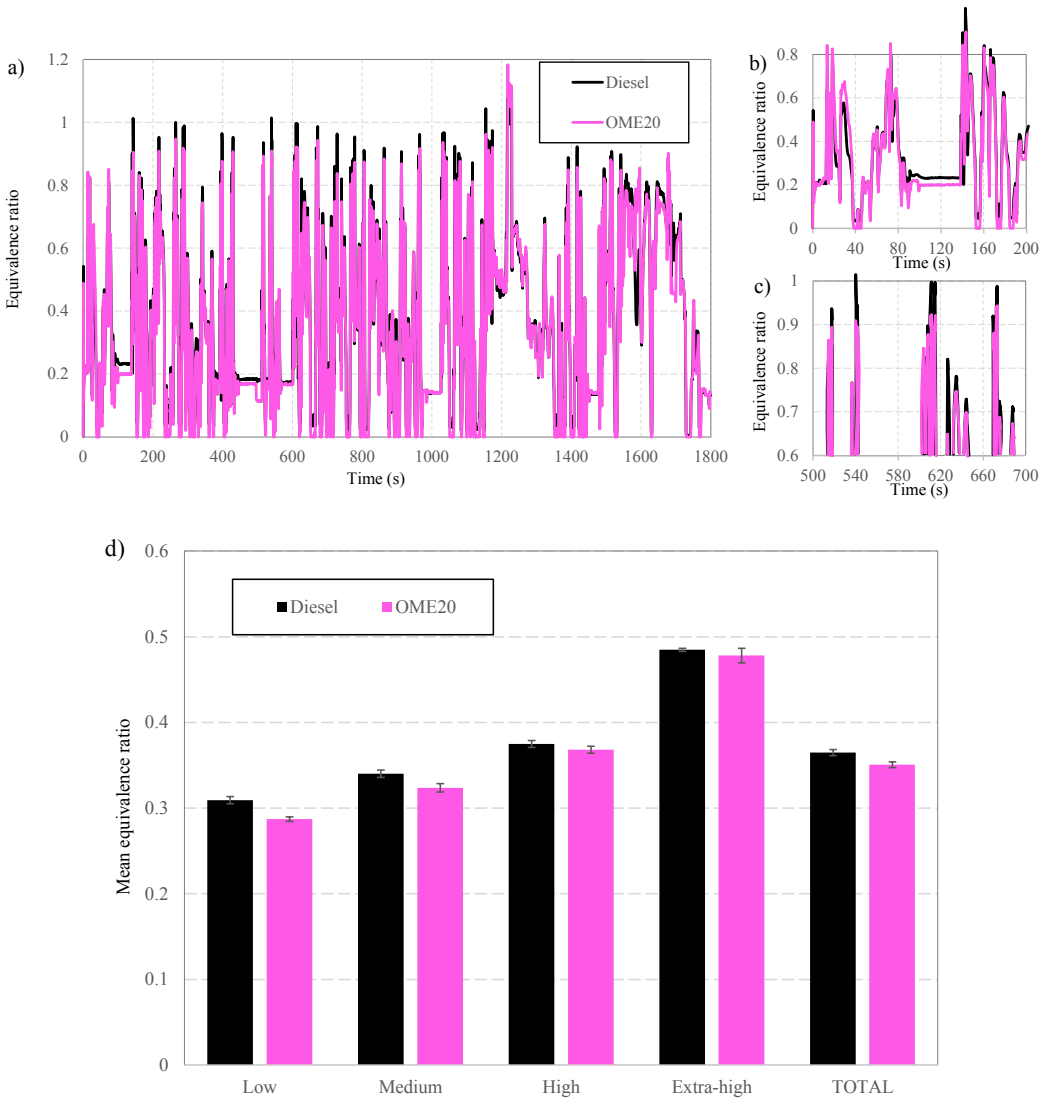

Fig. 4. Instantaneous equivalence ratio (a–c) and mean equivalence ratio (d) for each phase of the WLTC.

equivalence ratio (Fig. 4a) was high during accelerations and low at idle condition (although nil during decelerations). In both cases it decreased as the driving cycle progressed because the engine turned hotter. However, the mean equivalence ratio was significantly higher at high and extra high-speed driving cycle phases than at the previous phases, as observed in Fig. 4d. The instantaneous equivalence ratio higher than 1 at 1220 s corresponded to the LNT regeneration.

For the low and medium speed driving cycle phases, a slightly lower mean equivalence ratio was observed for OME20. This was especially noticeable at the initial idle period (Fig. 4b). However, in the high and extra high-speed driving cycle phases no significant differences were observed. It is worth to noting that the average differences shown in Fig. 4d derived mainly from specific acceleration points (see Fig. 4a and detailed example in Fig. 4c) in which the equivalence ratio was higher for diesel fuel. These high equivalence ratio points were closely related to particle number, THC and CO emissions, as discussed below. In most instants of high equivalence ratio, higher peaks were observed for diesel fuel.

Fig. 5 shows the instantaneous and mean EGR per each driving cycle phase, regardless of which EGR loop is active. At the beginning of the cycle only the HP-EGR is active (to avoid water condensation), and from around second 600 onwards LP-EGR is active instead. Engine emissions were markedly sensitive to the EGR rate, since small decreases in EGR lead to significant increases in NO formation and decreases in particle emissions, as discussed below. The EGR was inactive during both accelerations and decelerations. As the engine load increased, OME20 caused reduction in the EGR rate (Fig. 5a) due to its lower heating value which implied more fuel injection compared to diesel to reach the demanded power (Fig. 3a), thus modifying the accelerator position. This induced the EGR to decrease (Fig. 5c), either closing the EGR valves or opening the back-pressure valve, following the engine mapping strategy. Even more, during many accelerations, the EGR rate was nil for OME20 while it was not for diesel fuel (Fig. 5b), thus this explains the significant difference in the mean EGR rate per driving cycle phase (Fig. 5d).

3.2. Combustion diagnosis

Fig. 6 shows the average instantaneous in-cylinder pressure and the average heat release for each driving cycle phase. For OME20 the maximum combustion pressure was the highest (Fig. 6a), and both pressure rate and heat release rate peaks were advanced as the driving cycle progressed. Significant differences in heat release rate can be observed In Fig. 6b in both the pilot injection and the main injection, especially for high speeds. Due to the lower energy content of OME20, the amount of heat release during the pilot injection was lower compared to diesel. On the contrary, the peak of heat release rate in the

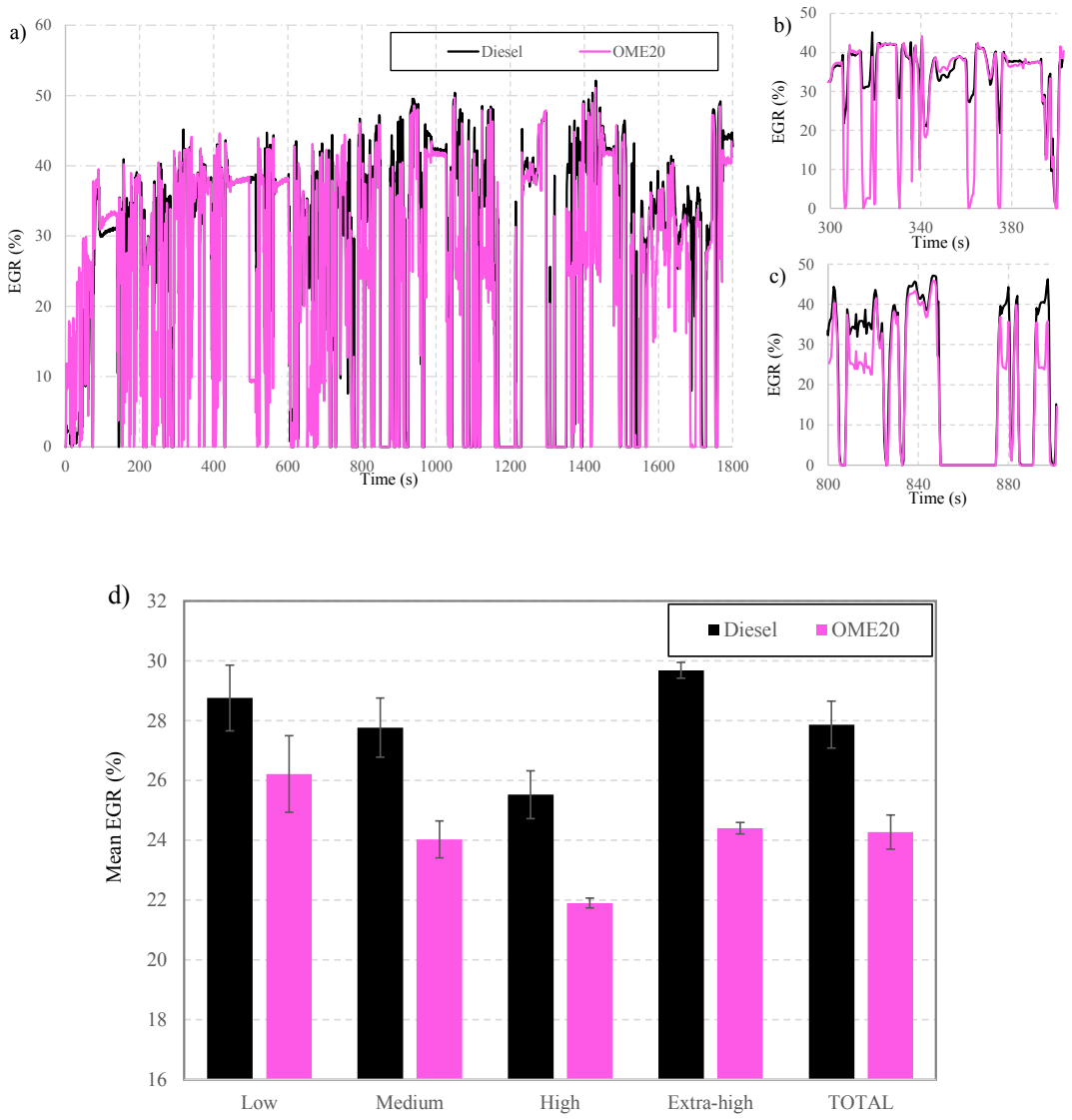

Fig. 5. Instantaneous exhaust gas recirculation rate (a–c) and mean exhaust gas recirculation (d) for each phase of the WLTC.

main injection was higher for OME20 than for diesel fuel, shortening the combustion duration, as shown in Fig. 6c (calculated as the difference between the crankangles for 10 % and 90 % of the final accumulated heat release).

It is believed that the OME's oxygen content and volatility promoted the combustion reaction leading to the increase of the burning rate, which increased the peak of heat release rate for OME20 compared to diesel fuel. This effect could also be partially attributed to the lower EGR rate for OME20, as mentioned above. In fact, the highest difference between pressure peaks was found in the extra high-speed driving cycle phase and the smallest difference was in the low-speed phase, coincidently with the difference in the EGR rate (Fig. 5a). The resulting shortened combustion duration would explain the increased brake thermal efficiencies.

3.3. Gaseous emissions

The gaseous emissions, including NO_x, CO and THC are shown in Figs. 7–9, respectively. Fig. 7 shows the instantaneous (left) and accumulated (right) emissions of nitrogen oxides (NO_x) and dioxide (NO_2). The NOx emissions varied considerably during the driving cycle. For both fuels, NO_x peaks were observed mainly during accelerations, because the EGR was not active since more fuel was injected. The highest differences in NO_x emission peaks and in the increasing rate of accumulated NOx emissions occurred in the medium-speed phase, corresponding to the highest EGR rate peaks (Fig. 5a).

The highest NO_x emissions for OME20 can be explained by both chemical and engine mapping effects. Chemical effects are related to fuel properties: both the oxygen content and high volatility facilitate oxygen-rich zones, which, together with high temperatures, promote the formation of NO. The engine mapping effects involve thermal and kinetic mechanisms. The thermal mechanism occurs because more OME20 fuel was required to achieve the demanded engine power. Thus, the accelerator pedal position was deeper, leading to lower EGR rate compared to diesel fuel (Fig. 5b). This caused an increase in local combustion temperature and consequently higher NO formation. Finally, the lower EGR rate of OME20 increased the combustion velocity (EGR is a flame retarder, as explained in [27]), leading to shorter combustion, and thus higher pressure and temperature peaks, which favored NO formation.

At the end of the driving cycle, OME20 increased NO_x emissions by 42 % with respect to diesel fuel. Similar differences in both instantaneous and accumulated NO_2 emissions were observed, indicating that NO/NO_2 ratio remained constant regardless the engine operating conditions.

Fig. 8 shows the CO instantaneous (left) and accumulated emissions

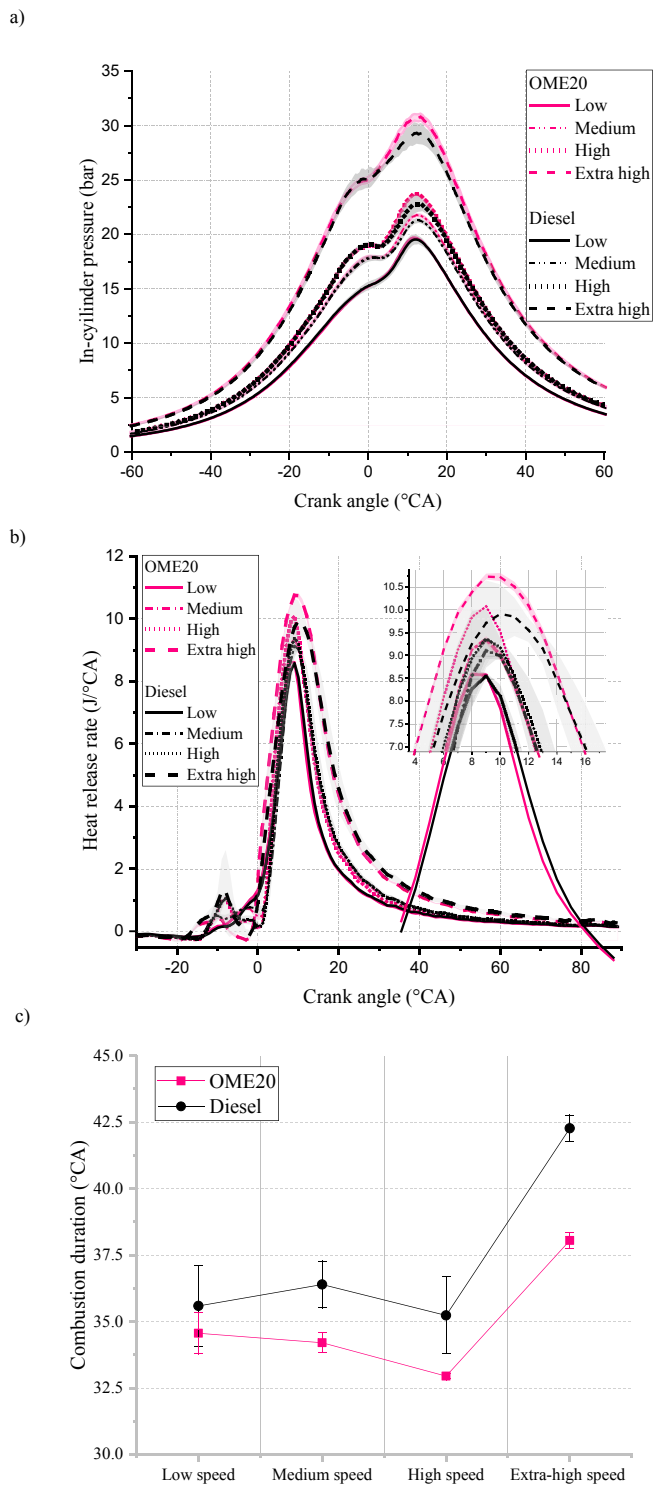

Fig. 6. Average in-cylinder pressure (a), heat release rate (b), and combustion duration (c) for each phase of the WLTC.

with both OME20 and diesel fuel. CO is mainly formed during cold-engine start conditions, since 58 % of the CO was emitted in the low-speed driving cycle phase for both fuels. Increasing load increased combustion temperature leading to higher conversion efficiency in the diesel oxidation catalyst. It is for this reason that accelerations such as those around second 1000 resulted in lower CO emissions than at seconds 280 and 600. Additionally, a sharp increase in accumulated CO emissions can be observed in second 1200, which was caused by the LNT regeneration. The addition of OME to diesel fuel resulted in a 52 % reduction in CO accumulated emissions compared to diesel because the additional oxygen in the fuel led to a better oxidation of CO to CO_2. When analyzing CO_2 emissions (not shown here), no significant differences were found between fuels, amounting around 2840 ± 40 g for both fuels at the end of the cycle.

Fig. 9 shows the THC instantaneous (left) and accumulated emissions for both tested fuels. THC emissions followed the same trend than CO. At the beginning of the cycle, in the low-speed driving cycle phase, high THC emissions were associated with low in-cylinder temperature. However, although both CO and THC emissions are related to cold engine conditions, one difference between them is that CO is more sensitive to accelerations, while THC are permanently emitted throughout the driving cycle. After approximately 1200 s of the cycle, there is a peak of emissions with both fuels due to the LNT regeneration.

With OME20 an additional LNT regeneration occurred in the latest part of the extra high-speed phase because NO_x emissions were high, therefore the LNT was saturated earlier than in the case of diesel, (as observed in Fig. 7) leading to an increase in THC emissions (Fig. 9). Such increase did not always take place at the same time in the cycle (either at second 1600 or at second 1680) which led to an apparent double peak of THC when averaging. This additional regeneration with OME20 partially compensated the reduction in THC emissions at the end of the cycle. Accumulated THC emissions were 17 % lower for OME20 than for diesel fuel. This decrease can be mainly explained by the reduction in EGR, and the lower equivalent ratio of OME20, which implied an excess of air, promoting a better THC and CO oxidation. However, it is likely that THC emissions were also influenced by the fuel formulation, since the oxygen content facilitated the combustion of fuel-rich areas, preventing the emission of unburned hydrocarbons.

3.4. Particle emissions

Fig. 10 shows both instantaneous and accumulated particle number (PN). The PN was higher in the acceleration periods, due to the higher equivalence ratio, resulting in a local lack of oxygen and poor combustion [28]. In these conditions, soot emissions increased and the solid particles in the accumulation mode increased. OME20 shows a marked effect on reducing PN compared to diesel fuel during the whole driving cycle, especially at the extra-high speed where the equivalence ratio is much higher. The total reduction in PN with OME20 was about 60 % and can be explained by both chemical effects and engine mapping strategy. Chemical effects are mainly related to the fuel formulation since OME20 has lower aromatic content, fewer C—C bonds, and much higher oxygen content (11 %) compared to neat diesel, thus promoting complete combustion and high in-cylinder temperature, which was favorable for soot oxidation. Previous studies have demonstrated that oxygenated fuels with higher number of C—C bonds promoted soot emissions even with similar oxygen content [29]. Regarding the engine mapping strategy, the deeper accelerator pedal position induced lower EGR rate (see Section 3.1), which may have the following implications: a) it increases the combustion velocity, leading to higher temperature peaks, favoring the oxidation of the soot (kinetic effects), b) it increases the oxygen concentration in the intake charge, reducing the formation of soot and facilitating its oxidation. However, such deeper pedal acceleration does not compensate the higher stoichiometric fuel/air ratio, leading to a leaner combustion condition. These effects enhanced the PN reduction, and together with the OME20 properties, reduced PN emissions more than other equally oxygenated fuels (11 % oxygen by weight) [30].

Fig. 11 shows that the trend of the number of particles in the nucleation mode decreased and shifted from bimodal mode to accumulation mode and upwards and towards larger size as the driving cycle progressed. The bimodal distribution was clearly separated into the nucleation mode with solid particles smaller than 23 nm (not regulated in Euro 5 and 6 standards) and the accumulation mode with solid particles larger than 23 nm (regulated). The particle size distribution

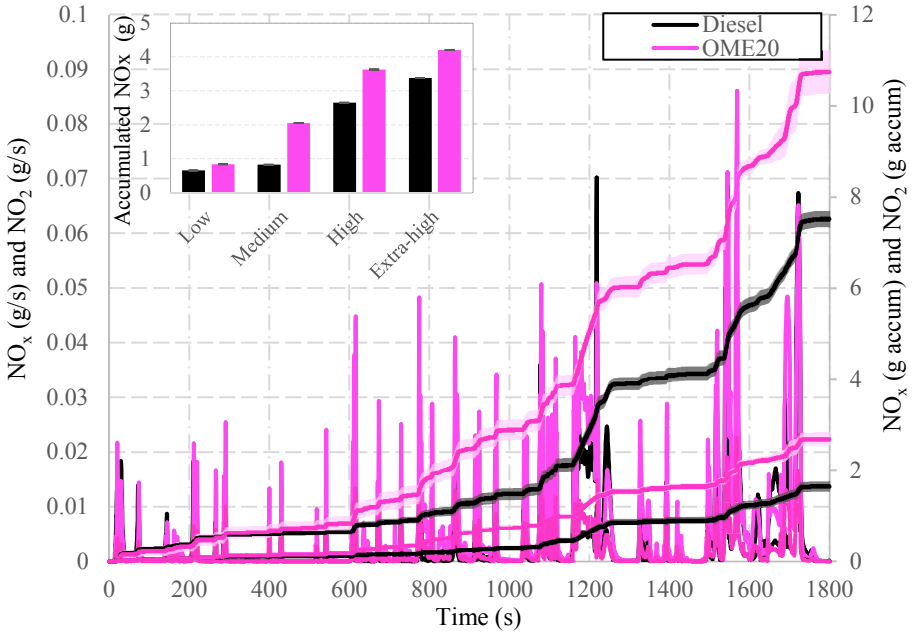

Fig. 7. NO_x and NO_2 emissions (left) instantaneous and (right) accumulated. Box inside represents the accumulated NO_x emissions per driving cycle phase of the WLTC.

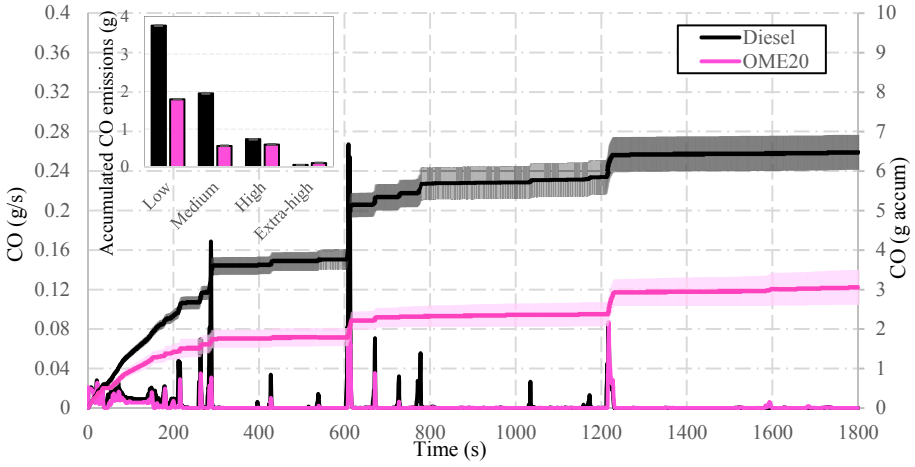

Fig. 8. CO emissions (left) instantaneous and (right) accumulated. Box inside represents the accumulated CO emissions per driving cycle phase of the WLTC.

showed a bimodal distribution at low-speed phase showing a distinctive nucleation mode with peak diameters around 9–10 nm, and an accumulation mode with peak diameters around 50–70 nm. This could be explained because when the engine is cold the amount of unburned hydrocarbons is high enough to saturate the soot particle surfaces by adsorption and heterogeneous nucleation, and subsequently favor homogeneous nucleation of small liquid particles [31]. As the cycle progresses, the in-cylinder temperature increased, and the unburned hydrocarbon emissions became relatively lower, and therefore the number of particles in the nucleation mode decreased.

OME20 decreased the peak number concentrations of accumulation-mode particles at low, medium, high, and extra high-speed driving cycle phases by 54.3 %, 39.7 %, 71.5 and 23 %, respectively, and caused a slight shift of the particles toward smaller size compared to diesel fuel. The oxygen content prevents from soot nucleation and promotes the oxidation of the already formed soot, leading to a decrease in the number and size in soot agglomerates. OME20 led to a sharp reduction in PN in the nucleation mode at low-speed phase (by 75 %), due to the higher volatility and lower viscosity of OME20, which would likely improve atomization, evaporation and air mixing in the combustion chamber compared to diesel fuel, thus limiting the nucleation of hydrocarbons. In this low-speed phase, diesel almost doubled the number of particles in the nucleation mode compared to those in the accumulation mode. For the rest of the cycle phases, OME20 exhibited a unimodal distribution in accumulation mode particles with a maximum particle size range between 45 and 70 nm. In contrast, diesel maintained a bimodal distribution in the low, medium, and high-speed phases.

Significant particle reductions have been reported when diesel-OME blends are used in internal combustion engines. Despite most studies do not make any changes to the engine mapping strategy, most authors attribute these reductions mainly to fuel properties, since OME fuel is composed of C—O—C bonds, and in the chemical mechanism reaction pathway, there is no direct way leading to olefin formation (C=C), which are important soot precursors [19]. In addition, its high oxygen content plays an important role in reducing soot. Liu et al. [11] reported up to 47.6 % smoke emission reduction with 30 % of OME blended with diesel. In a subsequent study [20], they showed a maximum reduction in the total PN of 28 % with the same OME blend. These reductions were

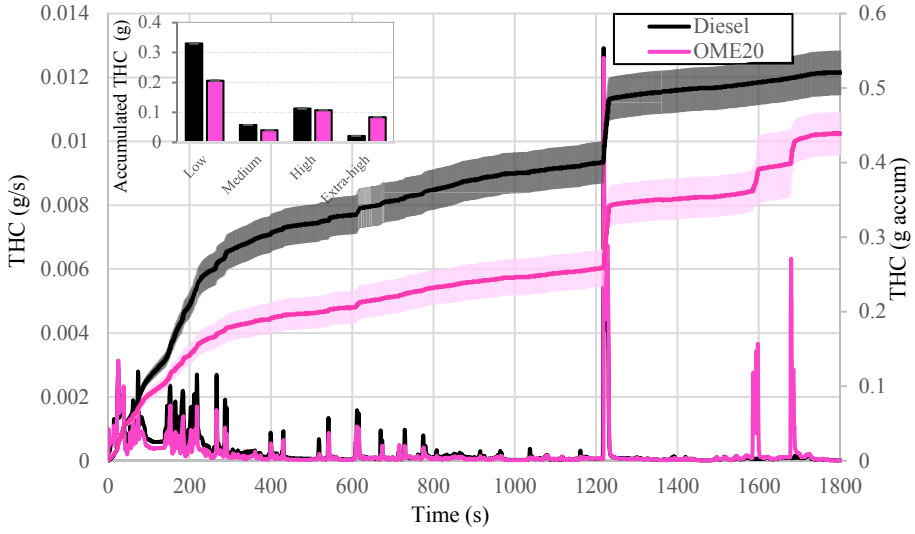

Fig. 9. THC emissions (left) instantaneous and (right) accumulated. Box inside represents the accumulated THC emissions per driving cycle phase of the WLTC.

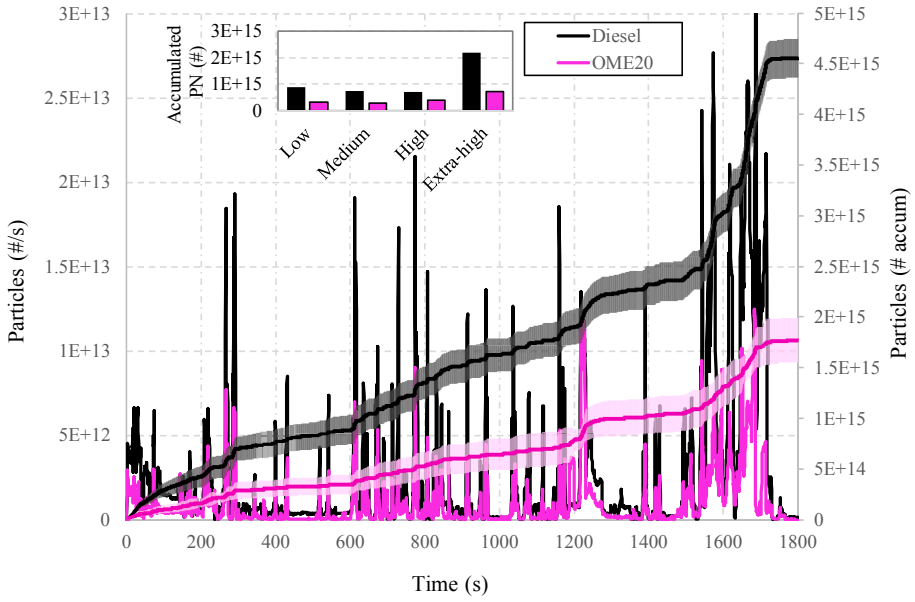

Fig. 10. PN instantaneous (left) and accumulated (right) emissions.

associated with the fuel compositional effects, such as the lack of C—C bonds and the intramolecular oxygen, the higher cetane number and the lower viscosity and boiling temperature which improved the interior fuel atomization making the combustion of air-fuel mixture faster than diesel fuel. The experiments were performed on a 4-cylinder turbocharged intercooled common-rail diesel engine, operating under steady state. Omari et al. [15] reported a particle matter reduction around 70–90 % with 35 % of OME. Such reduction was attributed to the high molecular oxygen content, which improved the local oxidation conditions, the high cetane number, as well as the higher burned mass fraction, leaving less fuel to be partially oxidized in the burn-out phase. The experiments were carried out in a single cylinder engine – 0.39L, at 5 different steady state operating points, maintaining constant the center of combustion for each load point and for all EGR rates. Wu et al. [14] showed a smoke opacity reduction up to 93 % by blending 25 % of OME with diesel in a L12 small agricultural engine. The higher oxygen content and no C—C bonds were the main reasons argued for the achieved soot reduction.

Based on the results of this study, it can be concluded that, besides the effects associated with the fuel chemical composition, the changes in the EGR rate and in the equivalence ratio derived from the engine mapping strategy have a significant impact on the change in regulated emissions relative to diesel. Therefore, an engine recalibration would allow to reduce NO_x emissions while partially sacrificing the reduction in PN. Additionally, since the LNT is not such an efficient system to reduce NO_x as the SCR-urea system, it could be expected that with an SCR system the increase in NO_x emissions would be lower, and therefore no or only minor recalibration would be required.

4. Conclusions

Experiments were conducted in a Euro 6 diesel engine under transient conditions fueled with diesel and its blend with 20 % by volume of OME (OME20). The effects of OME addition on engine performance, pollutant emissions (CO, NO_2, NO, THC, PN), and particle size distribution were investigated. It was observed that PN and regulated emissions, despite being strongly affected by the fuel properties (chemical effects), were markedly sensitive to EGR rate and equivalence ratio,

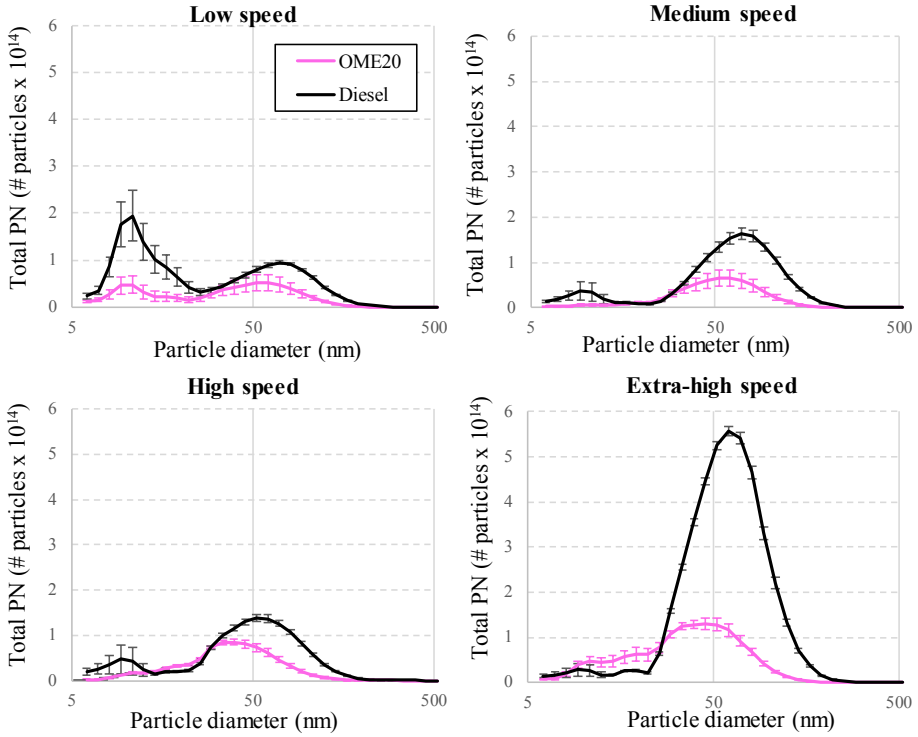

Fig. 11. Particle size distribution for each driving cycle phase.

which are preestablished in the engine mapping. Therefore, the following conclusions can be drawn:

- OME20 led to an increase in fuel consumption proportional to the reduced heating value. However, no significant differences in the total brake thermal efficiency were observed at the end of the driving cycle. The high efficiency at the initial phases was compensated by the low efficiency at the extra high-speed phase.
- OME20 led to lower EGR rate (even nil during many accelerations) compared to diesel, as a consequence of the specific engine mapping strategy.
- The lower EGR rate with OME20 (engine mapping effect), the oxygen content and the higher volatility (chemical effects) led to an increase of the burning rate, increasing the average in-cylinder pressure and heat release rate peaks, and consequently, shortening the combustion duration.
- NO_x emissions increased with OME20 as a consequence of different reasons: increase in the local combustion temperature due to lower EGR rate, and higher combustion velocity (engine mapping effects). In addition, the oxygen-rich zones due to the fuel-bound oxygen and the high local temperatures promote the formation of NO (chemical effects).
- Total THC and CO emissions were lower for OME20 than for diesel fuel due to a better oxidation of these pollutants derived from the lower equivalence ratio (engine mapping effects). THC emissions were also influenced by the oxygen content of the blend, which improves the combustion of fuel-rich areas and increases the efficiencies of the oxidation catalyst (chemical effects).
- The use of OME20 with 11 % oxygen in a Euro 6 engine, which has a specific mapping to maintain the NO_x-PM trade-off, reduced PN by 61 %. The combination of chemical reasons related to fuel formulation, together with engine mapping strategy, were responsible for this marked reduction in PN emissions.

CRediT authorship contribution statement

Silvana Arias: Investigation, Data curation, Writing – original draft. **John R. Agudelo:** Methodology, Supervision, Writing – review & editing. **Angel Ramos:** Investigation, Data curation, Validation. **Magín Lapuerta:** Resources, Conceptualization, Supervision, Writing – review & editing.

Declaration of Competing Interest

The authors declare that they have no known competing financial interests or personal relationships that could have appeared to influence the work reported in this paper.

Data availability

Data will be made available on request.

Acknowledgments

ChemCom Industries B.V (The Netherlands) is acknowledged for donating the OME fuel. The Ministry of Science, Technology and Innovation from Colombia is gratefully acknowledged by funding the program CAMBIO (Contract No. 80740-175-2021). Silvana Arias wishes to thank the financial support of Enlaza Mundos program – Sapiencia, Medellín municipality, call 2020 for financing the research internship.

References

[1] Zhao W, Yan J, Gao S, Lee TH, Li X. The combustion and emission characteristics of a common-rail diesel engine fueled with diesel, propanol, and pentanol blends under low intake pressures. Fuel 2022;307. https://doi.org/10.1016/j.fuel.2021.121692.
[2] Lapuerta M, Ramos Á, Barba J, Fernández-Rodríguez D. Cold- and warm-temperature emissions assessment of n-butanol blends in a Euro 6 vehicle. Appl Energy 2018;218:173–83. https://doi.org/10.1016/j.apenergy.2018.02.178.
[3] Blends D, Jamrozik A, Tutak W. Combustion stability, performance and emission characteristics of a CI engine fueled with Diesel/n-Butanol blends; 2021.

[4] Armas O, García-Contreras R, Ramos Á. Pollutant emissions from engine starting with ethanol and butanol diesel blends. Fuel Process Technol 2012;100:63–72. https://doi.org/10.1016/j.fuproc.2012.03.003.
[5] Transport and Environment. Electrofuels what role in EU transport decarbonisation? Eur Fed Transp Environ AISBL 2017:1–7.
[6] Burger J, Siegert M, Ströfer E, Nilles M, Hasse H. Poly(oxymethylene) dimethyl ethers as components of tailored diesel fuel – properties, synthesis and purification concepts. 11AIChE – 2011 AIChE Annu Meet Conf Proc 2011.
[7] Härtl M, Seidenspinner P, Jacob E, Wachtmeister G. Oxygenate screening on a heavy-duty diesel engine and emission characteristics of highly oxygenated oxymethylene ether fuel OME1. Fuel 2015;153:328–35. https://doi.org/10.1016/j.fuel.2015.03.012.
[8] Burger J, Ströfer E, Hasse H. Production process for diesel fuel components poly (oxymethylene) dimethyl ethers from methane-based products by hierarchical optimization with varying model depth. Chem Eng Res Des 2013;91:2648–62. https://doi.org/10.1016/j.cherd.2013.05.023.
[9] Drunsel J-O. Entwicklung von Verfahren zur Herstellung von Methylal und Ethylal 2012:162.
[10] Schmitz N, Burger J, Ströfer E, Hasse H. From methanol to the oxygenated diesel fuel poly(oxymethylene) dimethyl ether: An assessment of the production costs. Fuel 2016;185:67–72. https://doi.org/10.1016/J.FUEL.2016.07.085.
[11] Liu J, Sun P, Huang H, Meng J, Yao X. Experimental investigation on performance, combustion and emission characteristics of a common-rail diesel engine fueled with polyoxymethylene dimethyl ethers-diesel blends. Appl Energy 2017;202:527–36. https://doi.org/10.1016/j.apenergy.2017.05.166.
[12] Liu H, Wang Z, Wang J, He X, Zheng Y, Tang Q, et al. Performance, combustion and emission characteristics of a diesel engine fueled with polyoxymethylene dimethyl ethers (PODE3-4)/ diesel blends. Energy 2015;88:793–800. https://doi.org/10.1016/j.energy.2015.05.088.
[13] Wei Y, Zhang Y, Zhu Z, Zhu X, Gu H, Liu S. Effect of PODE on Emission Characteristics of a China VI Heavy-Duty Diesel Engine. Appl Sci 2022;12. https://doi.org/10.3390/app12031108.
[14] Wu S, Bao J, Wang Z, Zhang H, Xiao R. The regulated emissions and PAH emissions of bio-based long-chain ethers in a diesel engine. Fuel Process Technol 2021;214. https://doi.org/10.1016/j.fuproc.2021.106724.
[15] Omari A, Heuser B, Pischinger S, Rüdinger C. Potential of long-chain oxymethylene ether and oxymethylene ether-diesel blends for ultra-low emission engines. Appl Energy 2019;239:1242–9. https://doi.org/10.1016/j.apenergy.2019.02.035.
[16] Liu H, Wang Z, Zhang J, Wang J, Shuai S. Study on combustion and emission characteristics of Polyoxymethylene Dimethyl Ethers/diesel blends in light-duty and heavy-duty diesel engines. Appl Energy 2017;185:1393–402. https://doi.org/10.1016/j.apenergy.2015.10.183.
[17] Liu H, Ma X, Li B, Chen L, Wang Z, Wang J. Combustion and emission characteristics of a direct injection diesel engine fueled with biodiesel and PODE/biodiesel fuel blends. Fuel 2017;209:62–8. https://doi.org/10.1016/j.fuel.2017.07.066.
[18] Iannuzzi SE, Barro C, Boulouchos K, Burger J. POMDME-diesel blends: Evaluation of performance and exhaust emissions in a single cylinder heavy-duty diesel engine. Fuel 2017;203:57–67. https://doi.org/10.1016/j.fuel.2017.04.089.
[19] Wang T, Liu J, Sun P, Ji Q, Gao W, Yang C. Influence of injection parameters on combustion, gaseous emissions and particle size distribution of a CRDI diesel engine operating with PODE/diesel blends. Fuel 2020;281. https://doi.org/10.1016/j.fuel.2020.118733.
[20] Liu J, Liu Z, Wang L, Wang P, Sun P, Ma H, et al. Effects of PODE/diesel blends on particulate matter emission and particle oxidation characteristics of a common-rail diesel engine. Fuel Process Technol 2021;212. https://doi.org/10.1016/j.fuproc.2020.106634.
[21] Zhu Q, Zong Y, Yu W, Yang W, Kraft M. Understanding the blending effect of polyoxymethylene dimethyl ethers as additive in a common-rail diesel engine. Appl Energy 2021;300. https://doi.org/10.1016/j.apenergy.2021.117380.
[22] Liu J, Wang H, Li Y, Zheng Z, Xue Z, Shang H, et al. Effects of diesel/PODE (polyoxymethylene dimethyl ethers) blends on combustion and emission characteristics in a heavy duty diesel engine. Fuel 2016;177:206–16. https://doi.org/10.1016/j.fuel.2016.03.019.
[23] Preuß J, Munch K, Denbratt I. Performance and emissions of renewable blends with OME3-5 and HVO in heavy duty and light duty compression ignition engines. Fuel 2021;303. https://doi.org/10.1016/j.fuel.2021.121275.
[24] Rodríguez-Fernández J, Lapuerta M, Sánchez-Valdepeñas J. Regeneration of diesel particulate filters: Effect of renewable fuels. Renew Energy 2017;104:30–9. https://doi.org/10.1016/j.renene.2016.11.059.
[25] Lapuerta M, Armas O, García-Contreras R. Effect of ethanol on blending stability and diesel engine emissions. Energy Fuel 2009;23:4343–54. https://doi.org/10.1021/ef900448m.
[26] Zhao Y, Xie Y, Wang X, Li Z, Niu T, Liu S. Energy balance analysis, combustion characteristics, and particulate number concentration-NOx trade-off of a heavy-duty diesel engine fueled with various PODEn/diesel blends. Energy Convers Manag 2020;225. https://doi.org/10.1016/j.enconman.2020.113489.
[27] Qi D, Ma L, Chen R, Jin X, Xie M. Effects of EGR rate on the combustion and emission characteristics of diesel-palm oil-ethanol ternary blends used in a CRDI diesel engine with double injection strategy. Appl Therm Eng 2021;199. https://doi.org/10.1016/j.applthermaleng.2021.117530.
[28] Hountalas DT, Mavropoulos GC, Binder KB. Effect of exhaust gas recirculation (EGR) temperature for various EGR rates on heavy duty DI diesel engine performance and emissions. Energy 2008;33:272–83. https://doi.org/10.1016/j.energy.2007.07.002.
[29] Park W, Park S, Reitz RD, Kurtz E. The effect of oxygenated fuel properties on diesel spray combustion and soot formation. Combust Flame 2017;180:276–83. https://doi.org/10.1016/j.combustflame.2016.02.026.
[30] Shah AN, Yun-shan G, Shah FH, Mughal HU, Rahman ZU, Naveed A. Effect of biodiesel on particulate numbers and composition emitted from turbocharged diesel engine. Int J Environ Sci Technol 2014;11:385–94. https://doi.org/10.1007/s13762-013-0207-2.
[31] Merkisz J, Pielecha J. The process of formation of particulate matter in combustion engines. Springer Tracts Transp Traffic 2015;8:19–25. https://doi.org/10.1007/978-3-319-15928-7_3.